



Impact of Glass Irradiation on Laser-Induced Breakdown Spectroscopy Data Analysis

January 2023

Changing the World's Energy Future

Londrea J. Garrett, Bryan W. Morgan, Milos Burger, Yunu Lee, Hyeongbin Kim, Igor Jovanovic, Sungyeol Choi, Piyush Sabharwal



DISCLAIMER

This information was prepared as an account of work sponsored by an agency of the U.S. Government. Neither the U.S. Government nor any agency thereof, nor any of their employees, makes any warranty, expressed or implied, or assumes any legal liability or responsibility for the accuracy, completeness, or usefulness, of any information, apparatus, product, or process disclosed, or represents that its use would not infringe privately owned rights. References herein to any specific commercial product, process, or service by trade name, trade mark, manufacturer, or otherwise, does not necessarily constitute or imply its endorsement, recommendation, or favoring by the U.S. Government or any agency thereof. The views and opinions of authors expressed herein do not necessarily state or reflect those of the U.S. Government or any agency thereof.

Impact of Glass Irradiation on Laser-Induced Breakdown Spectroscopy Data Analysis

**Londrea J. Garrett, Bryan W. Morgan, Milos Burger, Yunu Lee, Hyeongbin Kim,
Igor Jovanovic, Sungyeol Choi, Piyush Sabharwall**

January 2023


**Idaho National Laboratory
Idaho Falls, Idaho 83415**

<http://www.inl.gov>

**Prepared for the
U.S. Department of Energy
Under DOE Idaho Operations Office
Contract DE-AC07-05ID14517**

Article

Impact of Glass Irradiation on Line Attenuation in Laser-Induced Breakdown Spectroscopy Diagnostics

Londrea J. Garrett ^{1,†} , Bryan W. Morgan ^{1,†}, Milos Burger ^{1,†}, Yunu Lee², Hyeongbin Kim³, Piyush Sabharwall⁴, Sungyeol Choi³, and Igor Jovanovic¹

¹ Department of Nuclear Engineering and Radiological Sciences, University of Michigan, Ann Arbor, MI 48109, United States; lgarr@umich.edu

² Department of Nuclear and Quantum Engineering, Korea Advanced Institute of Science and Technology, Daejeon 34141, Republic of Korea

³ Department of Nuclear Engineering, Seoul National University, Seoul 08826, Republic of Korea

⁴ Idaho National Laboratory, Idaho Falls, ID 83415, United States

* Correspondence: ijov@umich.edu

† Current address: Affiliation 1.

Abstract: Increased absorption of optical materials arising from exposure to ionizing radiation must be accounted for to accurately analyze laser-induced breakdown spectroscopy (LIBS) data retrieved from high-radiation environments. We evaluate this effect on specific examples that mimic the diagnostics placed within a gas-cooled fast reactor coolant stream and those placed within a molten salt reactor coolant stream. Analysis is performed on LIBS data measured with 1% Xe gas in an ambient He environment and 1% Eu in a LiCl-KCl matrix along with the measured optical absorption from the gamma- and neutron-irradiated low-OH fused silica and sapphire glasses. Significant changes in the number of shots required to reach a 3σ detection level was observed for the Eu data, increasing by two orders of magnitude after exposure to a 1.7×10^{17} n/cm² neutron fluence. Additionally for all cases examined, the spectral dependence of absorption results in either a systematic overestimation or underestimation of line intensity ratios, depending on the line of interest selected for analysis. Moreover, if lines from different spectral regions are used to create Boltzmann plots, this attenuation also leads to statistically significant changes in the temperatures calculated from the Xe II lines and Eu II lines, lowering them from 8000 ± 610 K to 6900 ± 810 K and from 15800 ± 400 K to 7200 ± 800 K respectively for the case of exposure to the 1.7×10^{17} n/cm² fluence. The temperature range required for 95% confidence interval for the calculated temperature is also broadened. In the case of measuring the Xe spectrum, these effects may be mitigated using only the longer-wavelength spectral region, where radiation-attenuation is relatively small, or through analysis using the iterative Saha-Boltzmann method.

Keywords: laser-induced breakdown spectroscopy (LIBS); gamma irradiation; neutron irradiation; advanced reactors; optical absorption

Citation: Garrett, L.J.; Morgan, B.W.; Burger, M.; Lee, Y.; Kim, H.; Sabharwall, P.; Choi, S.; Jovanovic, I. Impact of glass irradiation on line attenuation in laser-induced breakdown spectroscopy diagnostics. *Sensors* **2022**, *1*, 0. <https://doi.org/>

Received:

Accepted:

Published:

Publisher's Note: MDPI stays neutral with regard to jurisdictional claims in published maps and institutional affiliations.

Copyright: © 2022 by the authors. Submitted to *Sensors* for possible open access publication under the terms and conditions of the Creative Commons Attribution (CC BY) license (<https://creativecommons.org/licenses/by/4.0/>).

1. Introduction

There is significant current interest in the development of optical spectroscopy instrumentation for diagnostic applications in advanced reactor systems [1–5]. LIBS has been proposed as a candidate for instrumentation due to its multiple favorable characteristics, such as not requiring sample preparation, sensitivity to a wide range of materials, not requiring radioactive decay for detection, compatibility with analytes of arbitrary phase or composition, and ability to make remote measurements [6,7]. In LIBS, a high-power laser pulse, typically in the nanosecond range, is focused onto a sample and produces ionization through the mechanisms of multiphoton ionization and inverse bremsstrahlung [6,8]. In the context of reactor monitoring, researchers have proposed the inclusion of a LIBS module which can probe the reactor coolant stream and continuously track the composition [9].

The deployment of LIBS instrumentation in nuclear reactors will in many cases require that the optical components such as windows, lenses, and fibers be exposed to high doses of ionizing radiation. For successful LIBS implementation, these optics must remain optically transparent to both the excitation source (driving laser) as well as the plasma emission. It is well-known that optical materials such as glass experience damage at the atomic and molecular level that results in macroscopic changes to the material properties such as absorption and the change of refractive index [10–13]. If not accounted for, the altered material absorption could alter the perceived spectral line intensities when the plasma emission is transmitted through optics. Because these changes are nonuniform across the optical spectrum, more significant increases in absorption occur in the blue to UV spectral region.

Here, we present an analysis framework to predict the effects of irradiation on the analysis of the measured LIBS spectra. Calculations are performed based on the absorption data from recent irradiation studies [13,14] and two LIBS measurements meant to mimic conditions which may be observed in advanced reactor systems; a 1% Xe in an ambient He environment measurement relevant to gas-cooled fast reactor fuel cladding failure monitoring [2] and a 1% Eu in LiCl-KCl relevant to contamination monitoring in coolant streams and in pyroprocessing for molten salt reactors [5,15]. Due to the relatively small increases in absorption at the relevant Xe emission wavelengths, the detectability of individual spectral lines was found to be largely unaffected by 10-Mrad gamma irradiation for both the fused silica glass and sapphire. However, the more pronounced change of transmission induced by exposure to a combined neutron and gamma fluence results in a significant increase in the number of laser shots required for a statistically significant line intensity measurement. Equivalently, the strong attenuation predicted in the region where Eu emissions occur results in the number of shots required for statistical significance increasing for all irradiation conditions examined, with the mixed radiation fluence increasing this value by two orders of magnitude. The spectrally dependent nature of the transmission changes was also found to lead to significant errors in measuring both the Xe/He and Eu/Cl line intensity ratios and the extracted physical parameters such as plasma temperature, which can be calculated based on relative line intensities. However, if analysis can be focused to lines within the near infrared region, where the change of attenuation is small, the predicted effects are negligible. These results improve the understanding of the performance of LIBS systems exposed to large doses of ionizing radiation, which could extend their operational lifetime and increase time between instrumental calibrations.

2. Materials and Methods

2.1. Method and Calculation Details

The reduction in spectral line intensity is determined from the measured spectral absorption, quantified as the transmission T :

$$T = 10^{-D_A}, \quad (1)$$

where D_A is the absorbance in the units of optical density (OD). Using linear interpolation, the spectrally-dependent transmission is determined and multiplied by the measured spectrum. Due to relatively slow point-to-point variation in transmission as a function of wavelength, linear interpolation was determined to be a reasonable approximation for intermediate data points. Transmission spectra for the materials studied as a function of the radiation dose can be seen in Fig. 1. The effects studied in this work are separated into two categories: those impacted by a single spectral line and those impacted simultaneously by multiple spectral lines.

2.1.1. Single-Line Effects

Single-line detectability is characterized based on the signal-to-noise ratio (SNR), which is defined as

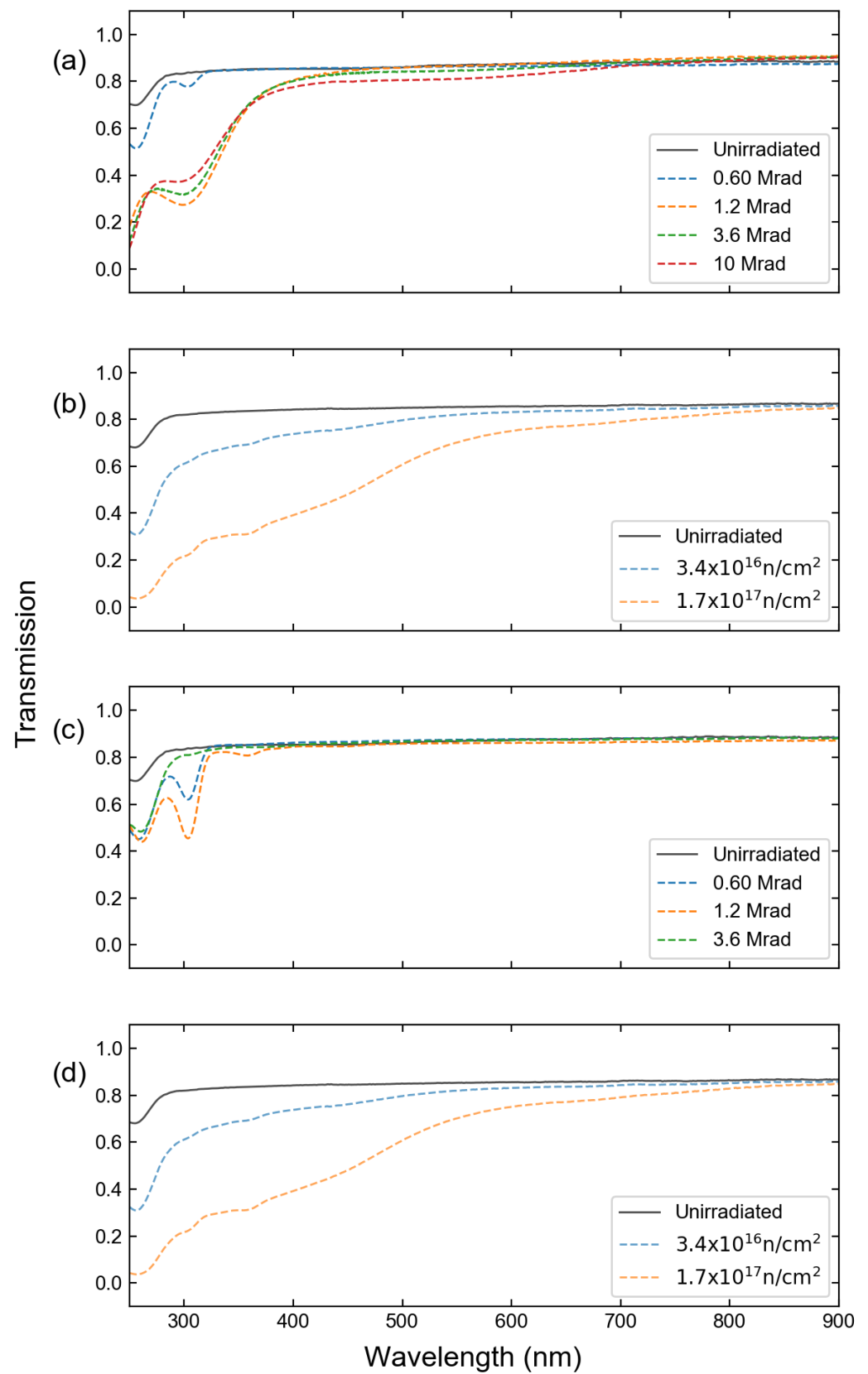


Figure 1. Transmission curves for (a) gamma-irradiated Infrasil-302, (b) neutron-irradiated Infrasil-302, (c) gamma-irradiated sapphire, and (d) neutron-irradiated sapphire windows.

$$SNR \equiv I_0/\sigma_B. \quad (2)$$

Here, I_0 is the intensity of the spectral line and σ_B is noise, corresponding to the standard deviation of the background. This value is calculated based on the spread observed in the region nearest the spectral line of interest that is devoid of spectral features over a wavelength range equal to the width of the line. The definition of standard deviation dictates that for a stable measurement, the SNR scales as

$$SNR = a N^{1/2}, \quad (3)$$

where a represents a fitting constant and N is the number of laser shots. Using this relation, the number of laser shots required to achieve a desired SNR can be estimated. For this study, the detectability limit is defined based on the 3σ criterion, such that lines are considered observable if their peak intensity is at least three times greater than the standard deviation of the background.

Both here and in all further calculations, the peak line intensity is determined by fitting a spectral line to a Voigt profile distribution [16–18], which is given by

$$\frac{I(\lambda)}{I_0} = \frac{2}{\pi} \frac{\lambda_0}{w_l} I_\lambda \int_{-\infty}^{\infty} \frac{\exp\left[-\frac{2.772\lambda_0^2}{w_g^2} \left(\frac{\nu}{c}\right)^2\right] d\left(\frac{\nu}{c}\right)}{1 + \frac{4}{w_l^2} [(\lambda - \lambda_0) - \lambda_0\left(\frac{\nu}{c}\right)]^2} + y_0. \quad (4)$$

Here, λ_0 is the wavelength at the line center, w_L is the Lorentzian half-width at half maximum (HWHM), w_G is the Gaussian HWHM, ν is the frequency, c is the speed of light, and y_0 is the vertical offset. The background is defined as a steady region near the peak that covers a span equal to the full-width at the base of the fitted peak as determined by Eq. (4). Once the number of shots required to reach the 3σ detection level is known, the time required is calculated by dividing the number of shots by the laser repetition rate. These calculations are performed with the original experimental data collected with a setup that was not exposed to ionizing radiation, and with the data adjusted for the radiation-induced attenuation.

2.1.2. Multi-Line Effects

Optical emission line ratios are commonly used to determine the relative component concentrations in a given elemental matrix [19]. Here, the ratio of both the Xe I and the Xe II line intensities were compared to that of the prominent He I line at 587.56 nm. Parameters such as the plasma temperature that can be used for normalization are commonly calculated using the relative line intensities of multiple spectral lines via the Boltzmann plot method [20–22]. In this study, we compare the standard Boltzmann plot method and the Saha-Boltzmann plot method as first described by Yalçin *et al.* [23] and later adapted by Aguilera and Aragón [24]:

$$\ln\left(\frac{I_0\lambda}{g_j A_{ij}}\right)^* = -\frac{1}{k_B T_p} E_j^* + \ln\left(\frac{N_0 h c}{Z(T_p)}\right) \quad (5)$$

In this expression, g_j is the upper level degeneracy, A_{ij} is the transition strength, k_B is the Boltzmann constant, T_p is the plasma temperature, E_j is the upper level energy, N_0 is the species number density, h is Planck's constant, c is the speed of light, and $Z(T)$ is the partition function. Asterisks denote quantities that must be adjusted for ionic transitions [23,24]. This method increases the accuracy through the inclusion of spectral lines across the ionization states. The assumption of local thermodynamic equilibrium (LTE) is supported by the McWhirter criterion,

$$n_e \gg 10^{19} \left(\frac{T_p}{e}\right)^{1/2} \left(\frac{\Delta E}{e}\right)^3, \quad (6)$$

as well as the measures described below. Here, n_e is the plasma electron density, e is the fundamental charge, and ΔE is the largest difference between subsequent energy levels. This relation describes the threshold at which the electron collision rates surpass radiative decay rates by a sufficient degree for LTE to be achieved [18,25]. It is assumed that Stark and instrumental broadening are the most significant contributors to spectral line broadening, allowing the plasma density to be calculated as

$$n_e = n_e^{ref} \left(\frac{\Delta\lambda}{w} \right)^{1/m}, \quad (7)$$

where n_e^{ref} is a reference electron density, $\Delta\lambda$ is the Lorentzian component of the spectral line FWHM as determined by Eq.(4), w is the line-specific Stark broadening parameter as found in literature, and m is a scaling parameter assumed to approximately equal to 1 [26]. If LTE or near LTE conditions exist, the plasma density value calculated using Stark broadening parameters should be in good agreement with the value calculated using the Saha-Eggert equation such that

$$n_e = 2 \frac{N_i}{N_j} \frac{Z_j(T_p)}{Z_i(T_p)} \left(\frac{m_e k_B T_p}{2\pi\hbar^2} \right)^{3/2} \exp \left(-\frac{E_\infty - \Delta E}{k_B T} \right).$$

Here, N_i is the atomic population of the i -th quantum state, $Z(T)$ is the partition function of the i -th quantum state, \hbar is the reduced Planck constant, E_∞ is the species ionization energy, and ΔE is a plasma correction factor [18]. Similar to the single-line effects, the multi-line effects are studied using the experimental LIBS data, which is then adjusted for radiation-induced attenuation.

2.2. Experiment

2.2.1. LIBS Data Collection

A schematic of the experimental setup used for the Xe LIBS measurement is shown in Fig. 2(a). The experimental cell contained a certified mixture of 0.994% Xe in He (99.999% purity) at room temperature and a pressure of 1.00×10^5 Pa (1.00 bar). Prior to filling, the cell was evacuated to a pressure of 10^{-5} Pa (10^{-7} mbar) to prevent contamination from air. A 1064-nm Nd:YAG laser (Surelite, Continuum) was focused into the cell by a 100-mm focal length lens to induce gas breakdown. The laser produced 10-ns, 250-mJ pulses at a repetition rate of 10 Hz. The resultant LIBS signal was collected using a collimator (CC52, Andor) and directed into an echelle spectrograph (Mechelle, Andor) through a 0.4-mm diameter optical fiber bundle. An intensified CCD (iStar T334, Andor) was used to record spectra. Timing between the CCD and laser was maintained using a digital delay generator (DG645, Stanford Research). A gate delay of 1 μ s was used to minimize the contribution of continuum radiation while still maintaining an environment conducive to LTE conditions. Additionally, a gate width of 1 μ s was selected, allowing for minimal spectral line variation over the collection time [25]. Each spectrum results from the accumulation of 20 laser shots. Wavelength calibrations were performed using an Ar lamp (Pen Light, Oriel).

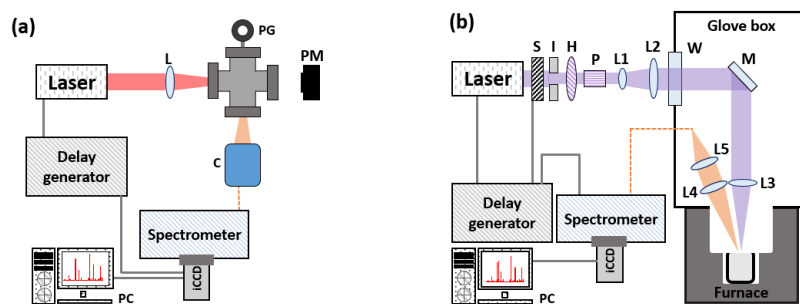


Figure 2. Setup for (a) the Xe in He and (b) the Eu in LiCl-KCl LIBS measurements [5]. L: Lens, PG: Pressure gauge, PM: Power meter, C: Collimator, S: Optical shutter, I: iris diaphragms, H: Half wave plate, P: Polarizer, W: Window, M: Laser line mirror.

Contrarily, the setup used for Eu measurements is shown in Fig. 2 (b). Measurements were performed inside a glove-box to maintain an ambient Ar environment. The experimental cell contained a mixture of 1.017% EuCl_3 in molten LiCl-KCl. Plasma was excited using a Nd:YAG laser operated at 266 nm (Q-smart with 2nd and 4th harmonic module, Quantel) with a pulse duration of 5 ns, pulse energy of 25 mJ, and repetition rate of 10 Hz. The beam was focused using a plano-convex lens with a focal length of 500 mm. Similarly to the Xe measurements, the signal produced was collected via optical fiber and transmitted to an Echelle spectrometer (Mechelle, Andor) coupled to an intensified CCD (iStar DH334T-18F-03, Andor) with timing regulated by a digital delay generator (DG645, Stanford Research). Spectra were measured with a gate width of 12.8 μs , gate delay of 0.500 μs , and resulted from the accumulation of 40 laser shots. Wavelength and intensity calibrations were performed with standard Hg and deuterium lamps respectively. Further detail on the measurement setup can be found in Ref. [5].

2.2.2. Absorption Measurements

The optical absorption was measured by irradiating the Infrasil-302 fused-silica glass and sapphire (Heraeus) in the dry tubes of the ^{60}Co irradiator located at the Nuclear Reactor Laboratory (Ohio State University) and in the water pools of the research reactor at the Radiation Science and Engineering Center (Pennsylvania State University). The glasses were selected due to their frequent use in optical components. For the gamma irradiation, the Infrasil-302 glass received a total dose of 10 Mrad, while the sapphire received a total dose of 3.6 Mrad. For the neutron irradiation, samples were exposed to combined neutron and gamma radiation with fluences of 3.4×10^{16} neutrons/ cm^2 and 1.7×10^{17} neutrons/ cm^2 , respectively. Absorption was measured using a broadband light source (DH-2000-BAL, Ocean Insight) and UV-NIR spectrometer (HR-4000 CG-UV-NIR, Ocean Insight). Further details on this measurement can be found in Ref. [13,14], where the irradiation conditions were carefully demonstrated and validated.

3. Results

Figure 3 shows the calculated effect on the Xe spectrum for light traversing a 1.2-cm thick window after receiving the maximum dosage for each irradiation method. Fig. 4 shows an equivalent comparison for the Eu measurement. Hereon, "gamma irradiation" denotes quantities affected due to the maximum dose received by the material during the gamma only irradiation while "neutron irradiation" denotes quantities affected by the highest combined gamma and neutron fluence. While all cases demonstrate more significant effects at shorter wavelengths, the exposure to high neutron fluxes is particularly detrimental for the detection of spectral lines in the important region of 250–500 nm, where the majority of Eu and Xe II emission is found. It can be noted, however, that minimal effects are observed in the near-infrared spectral region, where the Xe I spectral emission is located. While significant attenuation is unavoidable for Eu analysis, this suggests that it

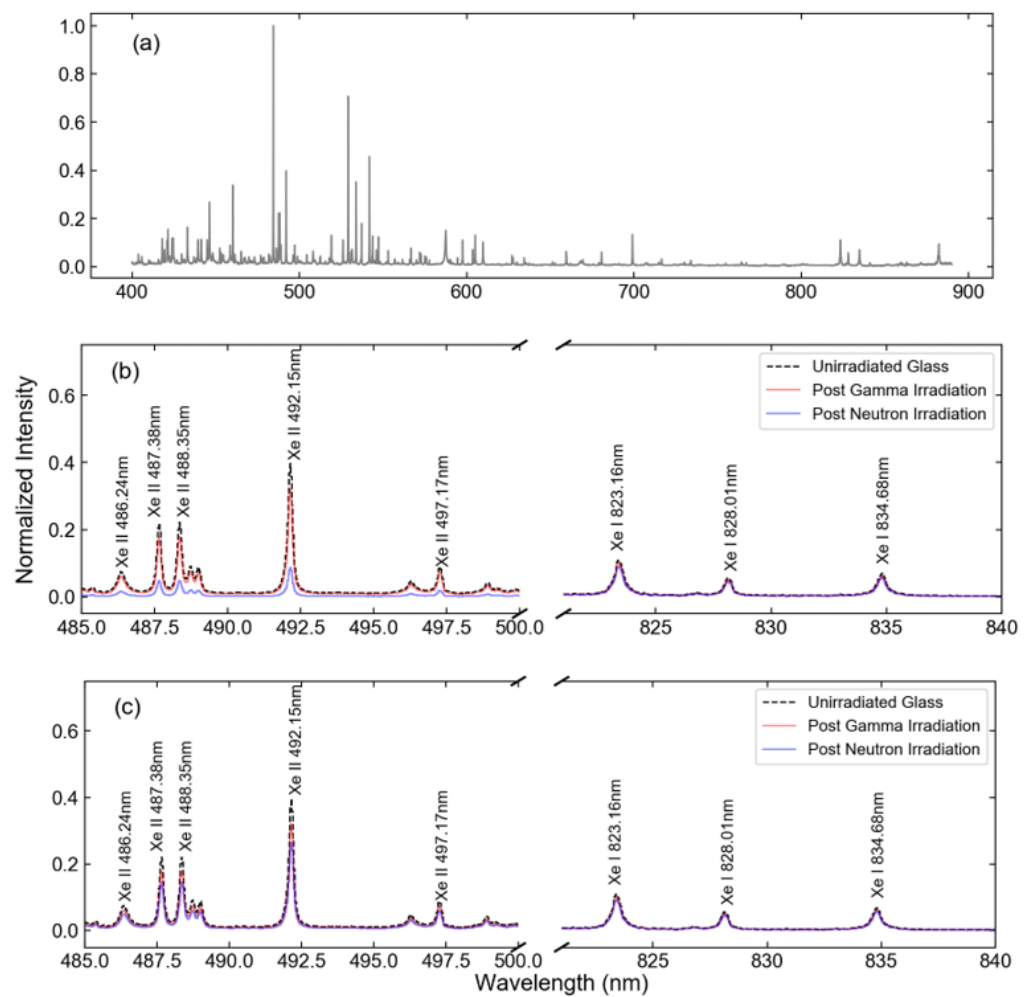


Figure 3. (a) Full measured 1% Xe in ambient He spectra and the spectra adjusted for the expected changes of absorption in (b) Infrasil-302 and (c) sapphire windows in the range of 485–500 nm and 825–840 nm

may be beneficial to base the Xe analysis primarily on the Xe I lines since the attenuation is nearly constant across the spectral range where those lines are located, and over 75% of the line intensity is maintained. Contrarily, this suggests that lines Eu II lines located below 300 nm are the least ideal for analysis as only 10–20% of light is transmitted after neutron irradiation.

Table 2 shows the changes to the single-line detectability as a function of received radiation dose for select Xe and Eu transitions, as calculated by Eq. 3 assuming constant scaling. For the gamma irradiations, the transmission of all lines over 400 nm remains above 75% for both tested materials, resulting in negligible changes to the number of laser shots required to meet the 3σ detection criterion for lines within this region. However, more significant attenuation was observed for lines located within the UV portion of the spectrum, particularly for Infrasil-302. In contrast, the line attenuation resulting from neutron damage leads to up to a $100\times$ increase in the minimum number of laser shots to meet the 3σ detection criterion for UV spectral lines and up to a $10\times$ increase for visible light spectral lines. Due to the high repetition rate available from modern laser systems, the required measurement time in these cases would remain tolerable. For example, for the laser used in this study that operates at a modest repetition rate of 10 Hz, all measurement times would remain on the order of minutes.

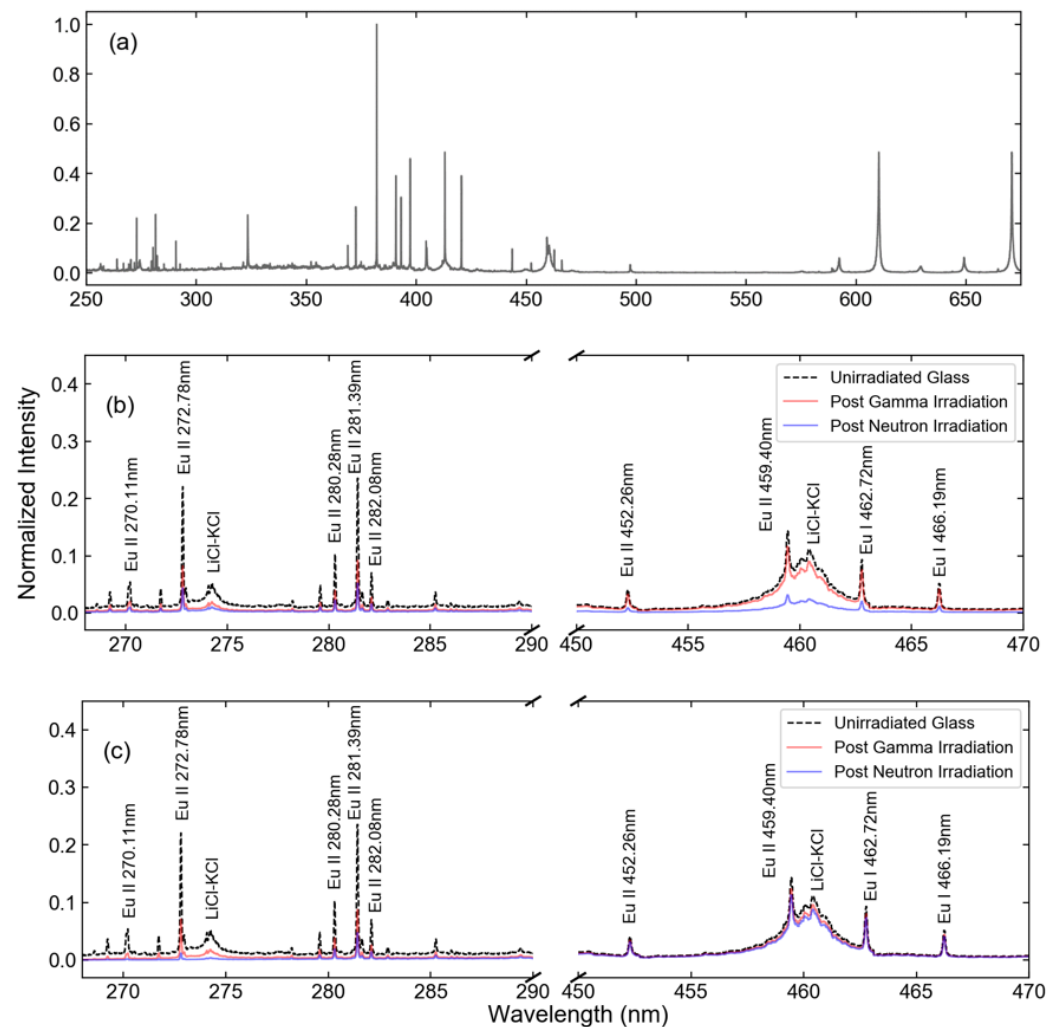


Figure 4. (a) Full measured 1% Eu in LiCl-KCl spectra and the spectra adjusted for the expected changes of absorption in (b) Infrasil-302 and (c) sapphire windows in the range of 270–290 nm and 450–470 nm. Features resulting from the molten salt background were the result of many closely spaced atomic transitions.

Figure 5 and Table 3 compare how the observed line intensity ratios for the Xe I 828.0-nm emission and Xe II 484.4-nm emission to the He I 587.6-nm as well as the Eu I 281.4-nm emission to the Li I 670.8-nm emission change for different window materials and radiation doses. Due to the increased attenuation at shorter wavelengths, the radiation-induced attenuation reduces the line intensity ratio for the short-wavelength Xe and Eu emissions and increases the line ratio for long-wavelength Xe emissions. Differences in material response can be attributed to radiation damage at molecular sites unique to that glass composition [13,14].

Boltzmann and Saha-Boltzmann plots are constructed by selecting the spectral lines that are resolvable, could be attributed to a single transition, and had relatively high upper level energies (Table 1) [30]. Figure 6 displays the calculated Boltzmann and Saha-Boltzmann plots for the Xe I and Xe II lines, while Figure 7 displays the Boltzmann and Saha-Boltzmann plots for both the original Eu data and the radiation-induced attenuation-corrected data. For both glasses, the presence of distinct transmission features leads to highly nonuniform attenuation across the spectrum, altering the temperature as calculated from the linear regression of Eq. 5. The LTE assumption is supported for the calculated plasma densities of $(2.25 \pm 0.35) \times 10^{17} \text{ cm}^{-3}$ and $(5.15 \pm 0.33) \times 10^{18} \text{ cm}^{-3}$ for Xe and Eu respectively, which meet the McWhirter Criterion [18,31]. The Xe value was calculated by

Table 1. Wavelength, transition probability, degeneracy, and upper and lower energy levels of selected Xe and Eu transitions according to NIST [27–29]

Species	Wavelength (nm)	Einstein coeff. (10^7s^{-1})	Lower level		Upper level	
			Degeneracy	Energy (eV)	Degeneracy	Energy (eV)
Xe I	764.202	2.1	1	9.4472	3	11.0691
	828.012	3.69	3	8.4365	1	9.9335
	834.682	4.2	3	9.5697	5	11.0547
	840.919	0.306	5	8.3153	3	9.7893
Xe II	433.052	14	6	14.0737	8	16.9360
	484.433	11	6	11.5390	8	14.0977
	487.650	6.3	6	13.5841	8	16.1259
	526.044	2.2	2	12.9254	4	15.2816
	526.195	8.5	4	14.0009	4	16.3565
	627.082	1.8	4	14.0009	6	15.9775
Eu I	311.143	3.3	8	0.0000	10	3.9836
	462.720	15.6	8	0.0000	8	2.6787
	466.188	15.2	8	0.0000	6	2.6588
Eu II	272.778	6.5	9	0.0000	11	4.5439
	281.393	5.5	9	0.0000	9	4.4048
	290.668	4.1	9	0.0000	7	4.2643
	372.490	4.5	9	0.0000	9	3.3276
	381.967	12.7	9	0.0000	11	3.2450
	397.190	8.9	7	0.2070	9	3.3276
	412.770	6.8	9	0.0000	9	3.0014
	420.505	7.1	9	0.0000	7	2.9476
	452.257	0.99	7	0.2070	7	2.9476

Table 2. The minimum number of laser shots for a 3σ detection level for the examined materials as a function of the irradiation method and received dose.

Spectral Line	Irradiation Condition	Shots for 3σ
Xe I, 828.0 nm	Unirradiated	1 ± 1
	Infrasil γ Irradiation	2 ± 2
	Infrasil n Irradiation	4 ± 2
	Sapphire γ Irradiation	1 ± 1
	Sapphire n Irradiation	1 ± 1
Xe II, 484.4 nm	Unirradiated	1 ± 1
	Infrasil γ Irradiation	2 ± 2
	Infrasil n Irradiation	17 ± 5
	Sapphire γ Irradiation	1 ± 1
	Sapphire n Irradiation	5 ± 3
Eu I, 462.7 nm	Unirradiated	4 ± 2
	Infrasil γ Irradiation	5 ± 3
	Infrasil n Irradiation	50 ± 7
	Sapphire γ Irradiation	5 ± 3
	Sapphire n Irradiation	13 ± 4
Eu II, 281.4 nm	Unirradiated	6 ± 3
	Infrasil γ Irradiation	36 ± 6
	Infrasil n Irradiation	131 ± 12
	Sapphire γ Irradiation	17 ± 5
	Sapphire n Irradiation	141 ± 12

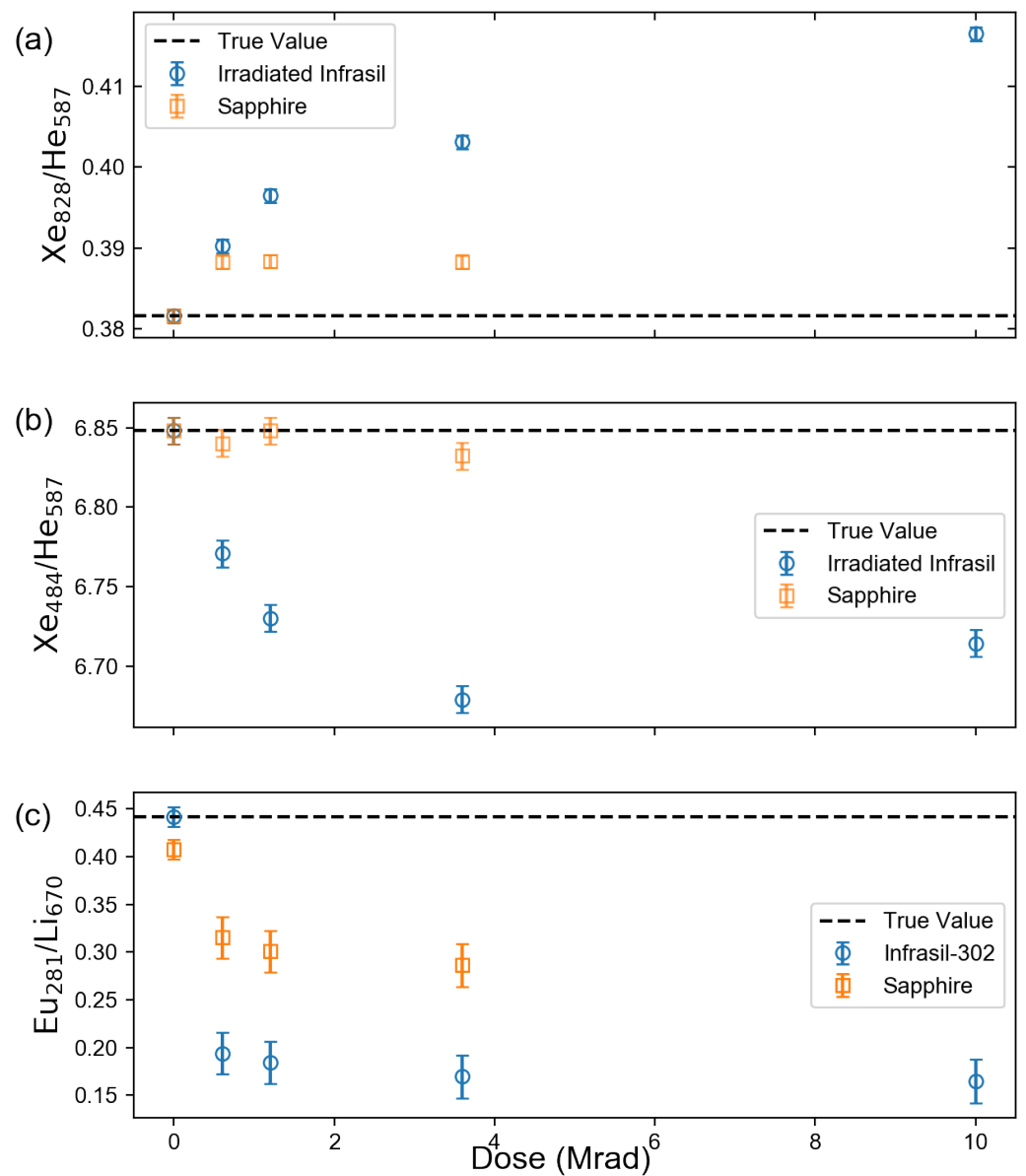


Figure 5. Gamma dose dependence of (a) intensity ratio of 828-nm Xe I line and 587-nm He I line; (b) intensity ratio of 484-nm Xe II line and 587-nm He I line; (c) intensity ratio of 281-nm Eu I line and 670-nm Li I line.

Table 3. Neutron fluence dependence of the line intensity ratios

Sample	Fluence (n/cm ²)	I ₈₂₈ /I ₅₈₇	I ₄₈₄ /I ₅₈₇	I ₂₈₁ /I ₆₇₀
Infrasil-302	0 (Unirradiated)	0.382±0.0008	6.74±0.008	0.571±0.01
	3.4×10 ¹⁶	0.497±0.0008	7.24±0.009	0.248±0.008
	1.7×10 ¹⁷	1.45±0.0009	9.46±0.009	0.123±0.004
Sapphire	0 (Unirradiated)	0.382±0.0008	6.84±0.008	0.513±0.01
	3.4×10 ¹⁶	0.509±0.0008	6.51±0.007	0.340±0.009
	1.7×10 ¹⁷	6.93±0.007	4.57±0.009	0.129±0.004

averaging the plasma density calculated individually for the 484.4 nm, 541.9 nm, 603.6 nm, and 605.1 nm lines associated with Xe II using the Stark data published by Konjevic [32,33] and the Lorentzian component of their respective FWHM values. The Eu value was

228
229
230

Table 4. Comparison of the calculated temperatures for both the Xe Boltzmann plots and Saha-Boltzmann plot

Method	Irradiation Condition	Temperature (K)	R ²
Xe I Boltzmann	Unirradiated	7810±390	0.9993
	Infrasil γ Irradiation	7770±390	0.9990
	Infrasil n Irradiation	7370±410	0.9909
	Sapphire γ Irradiation	7800±390	0.9992
	Sapphire n Irradiation	7740±400	0.9987
Xe II Boltzmann	Unirradiated	8000±610	0.9779
	Infrasil γ Irradiation	8000±850	0.9755
	Infrasil n Irradiation	8600±890	0.9960
	Sapphire γ Irradiation	8000±840	0.9759
	Sapphire n Irradiation	6900±880	0.9603
Eu II Boltzmann	Unirradiated	15800±400	0.9551
	Infrasil γ Irradiation	8900±400	0.9813
	Infrasil n Irradiation	9300±600	0.9164
	Sapphire γ Irradiation	13900±400	0.9473
	Sapphire n Irradiation	7200±800	0.9557
Xe Saha-Boltzmann	Unirradiated	7900±350	0.9983
	Infrasil γ Irradiation	8100±460	0.9981
	Infrasil n Irradiation	7660±500	0.9978
	Sapphire γ Irradiation	8000±410	0.9981
	Sapphire n Irradiation	8100±490	0.9981
Eu Saha-Boltzmann	Unirradiated	15200±400	0.9986
	Infrasil γ Irradiation	4400±500	0.9958
	Infrasil n Irradiation	4300±400	0.9947
	Sapphire γ Irradiation	4400±500	0.9926
	Sapphire n Irradiation	4300±400	0.9969

calculated analogously using the 397.2 nm and 420.5 nm lines associated with Eu II using Stark data from Popović et al. [34]. These values were found to be in good agreement with the density as calculated by the Saha-Eggert equation, Eq. (2.1.2). Error bars reflect the 95% confidence interval around the calculated temperature, as determined from the slope produced from linear regression. The changes in calculated temperature and the fit error resulting from attenuation corrections are shown in Table 4. When the Xe I lines alone are used, no significant change in temperature is noted due to the nearly uniform reduction in line intensities. As a result, the line slope from which the temperature is calculated remains nearly constant. In contrast, significant changes can be observed when only Xe II lines are used, since they are located in more strongly attenuated spectral regions and span a greater spectral range and this effect becomes even more pronounced for the Eu II lines. While the observed differences can be mitigated if the ionic line corrections are applied within the Saha-Boltzmann plot for Xe, the irradiation-induced attenuation acts to reduce the goodness of fit for the linear regression, as evidenced by the decrease in the associated R^2 value and increased fitting error. For Eu, while the temperatures determined once the irradiation effects are included are self-consistent, the temperatures predicted are not only significantly lower than the actual temperature, but are unrealistically low for a plasma to be sustained.

4. Discussion

Absorption data from the gamma and neutron irradiation of fused silica glass and sapphire windows was used to investigate the effect on the quantities derived from the analysis of LIBS spectra in which the emitted light travels through one of these materials. For a LIBS measurement of Xe in an ambient He environment, it was found that for

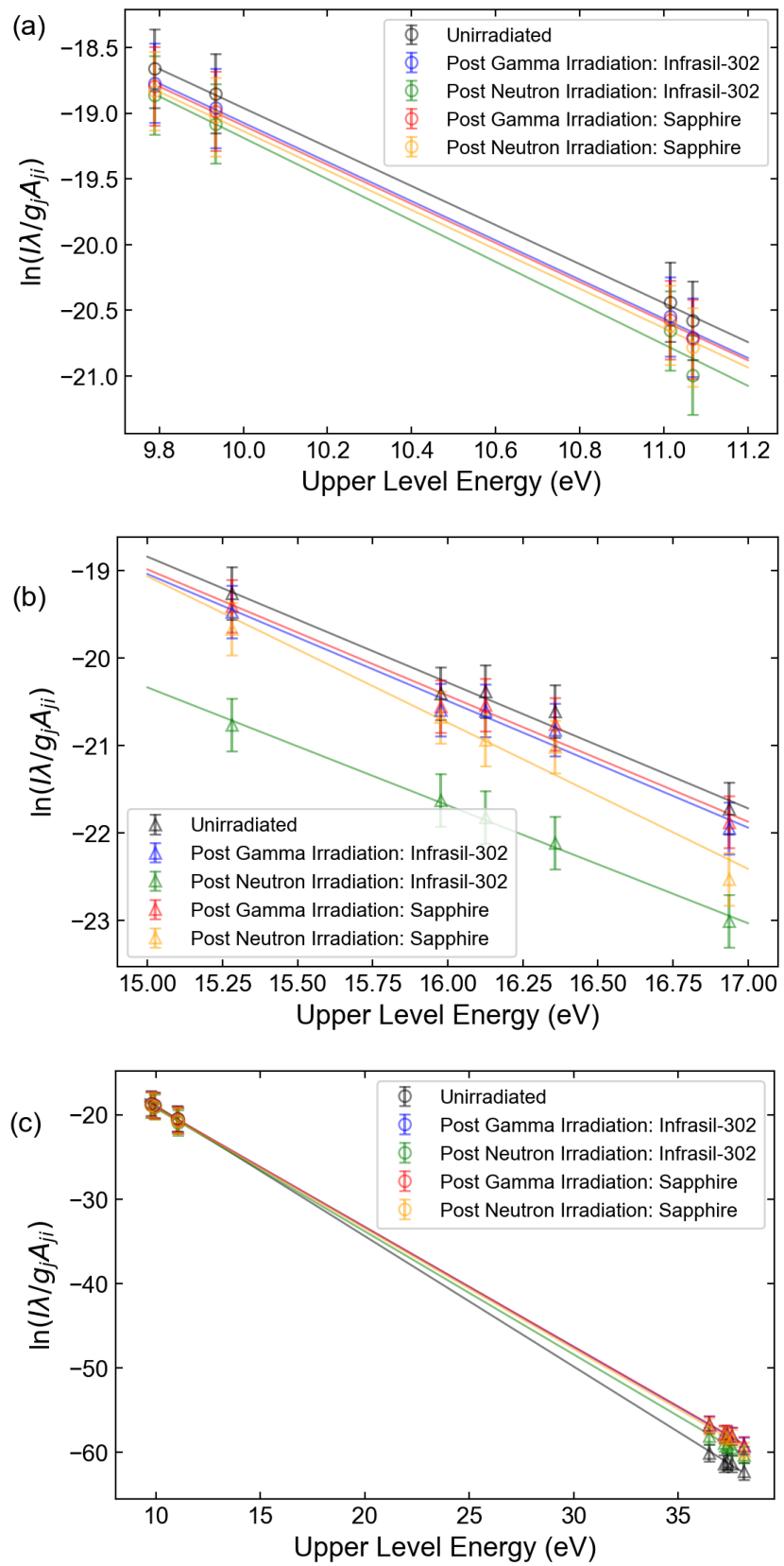


Figure 6. Boltzmann plots using the spectral data both before and after accounting for radiation-induced attenuation for (a) Xe I lines only, (b) Xe II lines only and (c) both groups combined using the Saha-Boltzmann method.

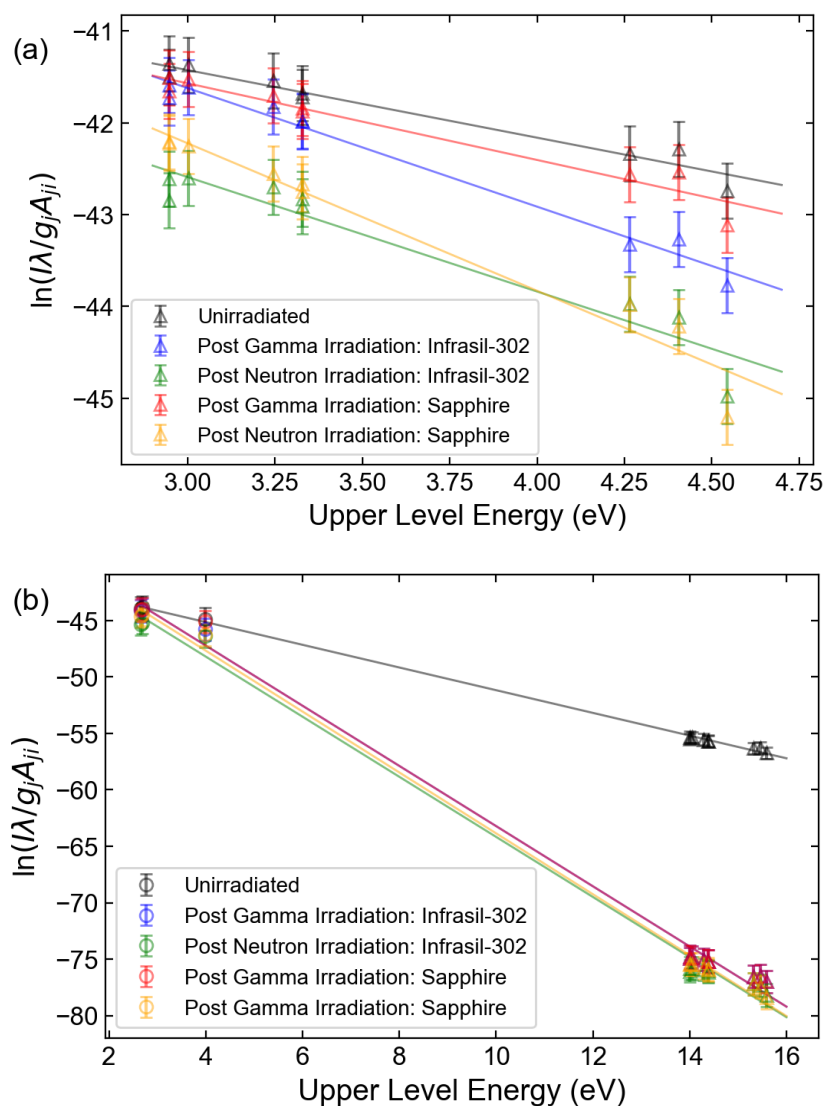


Figure 7. (a) Eu II Boltzmann plot and (b) Eu Saha-Boltzmann plot.

spectral lines which experience the most significant attenuation, the required number of laser shots to detect the line with the same statistical certainty increases by one order of magnitude, while the detectability of lines that are minimally attenuated remains largely unchanged. However, even at a modest repetition rate of 10 Hz, the measurement times in the investigated case remain relatively short, on the order of seconds. However, for a LIBS measurement of Eu in molten LiCl-KCl, the severe attenuation leads to a more significant increase, with the measurement time increasing from under a second to on the order of minutes. The effect of irradiation may be more pronounced if analysis were based on less prominent spectral lines. The nonuniform attenuation across the spectrum was found to have more noticeable effects on calculations that rely on the comparison of line intensity ratios, effectively overestimating the Xe/He and Eu/Li line ratios of shorter-wavelength Xe spectral lines such as the 484.4-nm Xe II and 281.9 nm Eu II lines respectively and underestimating the Xe/He line ratio of longer-wavelength Xe lines such as the 828.0-nm Xe I line. The nonuniform attenuation effect also manifests in the calculation of temperature using Boltzmann plots such that the error on the resultant temperature value increases.

The results of this study suggest that the changes error in calculations introduced from radiation-induced attenuation may be negligible or mitigated through the introduction of additional calibrations for spectral lines of interest to helium-cooled fast reactors. However,

it must be noted that the Xe concentration used is significantly greater than what would be expected within a reactor coolant stream during standard operation. Similarly, the concentration of Eu used in this study greatly exceeds what would be present within realistic measurement conditions in molten salt reactors. This likely greatly improves the predicted single-line detectability. To more accurately predict the effects within a reactor environment, the same analysis could be applied to a spectrum resulting from ppm to ppb concentrations of the analyte of interest as well as spectra that include other expected fission fragments to help account for matrix effects [19,35]. In addition, studies suggest that effects of thermal annealing, which may occur concurrently within the glass, depending on the proximity to the reactor high temperatures of the reactor core, can repair some of the radiation damage observed [13,14]. Therefore, corrections must also consider the these effects. Other future work may include the analysis of spectra relevant to LIBS in other high-radiation environments such as for spent fuel cask monitoring [36].

Declaration of Competing Interests

The authors declare that they have no known competing financial interests or personal relationships that could have appeared to influence the work reported in this paper.

Author Contributions: Conceptualization, I.J. and S.C.; methodology, M.B., I.J., and L.G.; formal analysis, L.J., Y.L., M.B., B.M., and H.K.; resources, P.S. and I.J.; funding acquisition, P.S., S.C., and I.J. All authors were involved in writing, review, and editing of the manuscript. All authors have read and agreed to the published version of the manuscript.

Funding: This work was supported by the Department of Energy, Nuclear Science User Facilities (DE-NE0008906); U.S. Department of Defense (HDTRA1-20-2-0002); B. W. M (Army Advanced Civil Schooling Program).

This work was conducted in conjunction with the Versatile Test Reactor project and is based upon work supported by the U.S. Department of Energy under Prime Contract No. DE-AC07-05ID14517 to the Idaho National Laboratory. Any opinions, findings, and conclusions or recommendations expressed in this publication are preliminary and are those of the author(s) and do not necessarily reflect the views of the U.S. Department of Energy or the Idaho National Laboratory.

This research was performed under appointment to the Nuclear Nonproliferation International Safeguards Fellowship Program sponsored by the Department of Energy, National Nuclear Security Administration's Office of International Nuclear Safeguards (NA-241).

This work was also supported by the National Research Foundation of Korea (NRF) funded by the Ministry of Science and ICT (grant numbers: 2020M2A8A1000972 and 2022M2D4A1052797).

Data Availability Statement: The data that support the findings of this study are available from the corresponding author upon reasonable request.

Acknowledgments: This research was performed under appointment to the Nuclear Nonproliferation International Safeguards Fellowship Program sponsored by the Department of Energy, National Nuclear Security Administration's Office of International Nuclear Safeguards (NA-241).

Conflicts of Interest: The authors declare no conflict of interest. The funders had no role in the design of the study; in the collection, analyses, or interpretation of data; in the writing of the manuscript; or in the decision to publish the results.

Abbreviations

The following abbreviations are used in this manuscript:

NIR	Near Infrared
UV	Ultraviolet
LIBS	Laser-induced breakdown spectroscopy
SNR	Signal to Noise Ratio
HWHM	Half-width at half maximum
Nd:YAG	Neodymium-doped yttrium aluminum garnet
ppm	parts per million
ppb	parts per billion

References

- Williams, A.; Phongikaroon, S. Laser-induced Breakdown Spectroscopy (LIBS) Measurement of Uranium in Molten Salt. *Appl. Spectrosc.* **2018**, *72*, 1029–1039.
- Burger, M.; Garrett, L.; Burak, A.; Petrov, V.; Manera, A.; Sabharwall, P.; Sun, X.; Jovanovic, I. Trace xenon detection in helium via laser-induced breakdown spectroscopy. *J. Anal. At. Spectrom.* **2021**, *36*, 824–828.
- Andrews, H.; Myhre, K. Quantification of Lanthanides in a Molten Salt Surrogate Off-Gas Stream Using Laser-Induced Breakdown Spectroscopy. *Appl. Spectrosc.* **2022**.
- Andrews, H.; MacFarlane, J.; Myhre, K. Monitoring Noble Gases (Xe and Kr) and Aerosols (Cs and Rb) in a Molten Salt Reactor Surrogate Off-Gas Stream Using Laser-Induced Breakdown Spectroscopy (LIBS). *Appl. Spectrosc.* **2022**.
- Lee, Y.; Yoon, S.; Kim, N.; Kang, D.; Kim, H.; Yang, W.; Burger, M.; Jovanovic, I.; Choi, S. In-situ measurement of Ce concentration in high-temperature molten salts using acoustic-assisted laser-induced breakdown spectroscopy with gas protective layer. *Nucl. Eng. Technol.* **2022**, *in press*.
- Cremers, D.; Radziemski, L. *Handbook of Laser-Induced Breakdown Spectroscopy*; John Wiley Sons: New Jersey, 2013.
- Russo, R.; Mao, X.; Gonzalez, J.; Zorba, V.; Yoo, J. Laser Ablation in Analytical Chemistry. *Anal. Chem.* **2013**, *85*, 6162–6177.
- Rusak, D.; Castle, B.; Smith, B.; Winefordner, J. Fundamentals and Applications of Laser-Induced Breakdown Spectroscopy. *Crit. Rev. Anal. Chem.* **1997**, *27*, 257–290.
- Sabharwall, P.; Weaver, K.; Anand, N.; Ellis, C.; Sun, X.; Choi, H.; Chen, D.; Christensen, R.; Fronk, B.; Gess, J.; et al. Preconceptual Design of Multifunctional Gas-Cooled Cartridge Loop for the Versatile Test Reactor: Instrumentation and Measurement—Part II. *Nucl. Sci. Eng.* **2022**, *196*, 215–233.
- Primak, W.; Edwards, E. Radiation-induced dilations in vitreous silica. *Phys. Rev.* **1962**, *128*, 2580–2588.
- Primak, W.; Luthra, J. Radiation induced expansion and increase in refractive index of magnesium oxide; evidence for the F center. *Phys. Rev.* **1966**, *39*, 5651–5658.
- Sharma, G.; Thind, K.; Manupriya.; Klare, H.; Narang, S.; Gerward, L.; Dangwal, V. Effects of gamma-ray irradiation on optical properties of ZnO-PbO-B₂O₃ glasses. *Nucl. Instrum. Methods Phys. Res. B* **2006**, *243*, 345–348.
- Morgan, B.; Van Zile, M.; Sabharwall, P.; Burger, M.; Jovanovic, I. Gamma-radiation-induced negative nonlinear absorption in quartz glass. *Opt. Mater. Express* **2022**, *36*, 1188–1197.
- Morgan, B.; Van Zile, M.; Petrie, C.; Sabharwall, P.; Burger, M.; Jovanovic, I. Optical Absorption of Fused Silica and Sapphire Exposed to Neutron and Gamma Radiation with Simultaneous Thermal Annealing. *J. Nucl. Mater.* **2022**, *507*.
- Yoo, J.; Seo, C.; Kim, E.; Lee, H. A conceptual study of pyroprocessing for recovering actinides from spent oxide fuels. *Nucl. Eng. Technol.* **2008**, *40*, 581–592.
- Tudor, D.; Vaughan, J. A New Tabulation of the Voigt Profile. *Astrophys. J.* **1963**, *137*, 1302–1305.
- Whiting, E. An empirical approximation to the Voigt profile. *J. Quant. Spectrosc. Radiat. Transfer* **1968**, *8*, 1379–1384.
- Griem, H. *Principles of Plasma Spectroscopy*; Cambridge University Press: New York, 1997.
- El Haddad, J.; Canioni, L.; Bousquet, B. Good practices in LIBS analysis: Review and advices. *Spectrochim. Acta B: At. Spectrosc.* **2014**, *101*, 171–182.
- Essien, M.; Radziemsky, L.; Sneddon, J. Detection of cadmium, lead and zinc in aerosols by laser-induced breakdown spectrometry. *J. Anal. At. Spectrom.* **1988**, *3*, 985–988.
- Joseph, M.; Xu, N.; Majidi, V. Time-resolved emission characteristics and temperature profiles of laser-induced plasmas in helium. *Spectrochim. Acta B: At. Spectrosc.* **1994**, *49*, 89–103.
- Aragón, C.; Peñalba, F.; Aguilera, J. Spatial characterization of laser-induced plasmas: distributions of neutral atom and ion densities. *Appl. Phys. A* **2004**, *79*, 1145–1148.
- Yalçın, Ş.; C.D.; Smith, G.; Faris, G. Influence of ambient conditions on the laser air spark. *Appl. Phys. B* **1999**, *68*, 121–130.
- Aguilera, J.; Aragón, C. Mult-element Saha-Boltzmann and Boltzmann plots in laser-induced plasmas. *Spectrochim. Acta B: At. Spectrosc.* **2007**, *62*, 378–385.
- Cristoforetti, G.; De Giacomo, A.; Dell’Aglia, M.; Legnaioli, S.; Tognoni, E.; Palleschi, V.; Omenetto, N. Local Thermodynamic Equilibrium in Laser-Induced Breakdown Spectroscopy: Beyond the McWhirter criterion. *Spectrochim. Acta B: At. Spectrosc.* **2010**, *65*, 86–95.
- Burger, M.; Hermann, J. Stark broadening measurements in plasmas produced by laser ablation of hydrogen containing compounds. *Spectrochim. Acta B: At. Spectrosc.* **2016**, *122*, 118–126.
- Sabbagh, J.; Sadeghi, N. Experimental transition probabilities of some Xe(I) lines. *J. Quant. Spectrosc. Radiat. Transfer* **1977**, *17*, 297–301.
- Shuker, R.; Binur, Y.; Szöke, A. Studies of afterglow in noble-gas mixtures: A model for energy transfer in He/Xe. *Phys. Rev. A* **1975**, *12*.
- Fuhr, J.; Wiese, W. *CRC Handbook of Chemistry and Physics*, 79th ed.; CRC Press: Boca Raton, Florida, 1998.
- Sun, L.; Yu, H. Correction of self-absorption in calibration-free laser-induced breakdown spectroscopy by an internal reference method. *Talanta* **2009**, *79*, 288–395.
- Hutchinson, I. *Principles of Plasma Diagnostics*, 2nd ed.; Cambridge University Press: New York, 2002.
- Konjevic, N.; Dimitrijevic, M.; Wiese, W. Experimental Stark Widths and Shifts for Spectral Lines and Neutral Atoms (A Critical Review of Selected Data For the Period 1976 to 1982. *J. Phys. Chem. Ref. Data* **1984**, *13*, 619–647.

-
33. Konjevic, N.; Lesage, A.; Fuhr, J.; Wiese, W. Experimental Stark Widths and Shifts for Spectral Lines of Neutral and Ionized Atoms (A Critical Review of Selected Data for the Period 1989 Through 2000). *J. Phys. Chem.* **2002**, *31*, 819–927. 376 377
34. Popovic, L.; Dimitrijevic, M.; Ryabchikova, T. The electron-impact broadening effect in CP stars: the case of La II, La III, Eu II, and Eu III lines. *AA* **1999**, *350*, 719–724. 378 379
35. Hahn, D.; Omenetto, N. Laser-Induced Breakdown Spectroscopy (LIBS), Part I: Review of Basic Diagnostics and Plasma-Particle Interactions: Still-Challenging Issues Within the Analytical Plasma Community. *Appl. Spectrosc.* **2010**, *64*, 335A–366A. 380 381
36. Xiao, X.; Le Berre, S.; Fobar, D.; Burger, M.; Skrodzki, P.; Hartig, K.; Motta, A.; Jovanovic, I. Measurement of chlorine concentration on steel surfaces via fiber-optic laser-induced breakdown spectroscopy in double-pulse configuration. *Spectrochim. Acta B: At. Spectrosc.* **2018**, *141*, 44–52. 382 383 384